

Evolution to quasi-equilibrium studied through decoherence of multiple-quantum coherence NMR spectra.

H. H. Segnorile, C. E. González and R. C. Zamar

*Instituto de Física Enrique Gaviola - CONICET, Facultad de Matemática,
Astronomía y Física, Universidad Nacional de Córdoba*

M.Allende y H. de la Torre - Ciudad Universitaria, X5016LAE - Córdoba, Argentina

(Dated: January 3, 2017)

We present a Nuclear Magnetic Resonance experiment aimed to scan the evolution of a spin system, in liquid crystals, during the transient to a quasi-equilibrium state. New evidence is presented in favor of irreversible decoherence as the mechanism which leads an initial out-of-equilibrium state to quasi-equilibrium. The experiment combines the Jeener-Broekaert sequence with reversal of the dipolar evolution, and decoding of multiple quantum coherences, to allow visualizing the evolution of the spectra of the different coherences during the formation of the quasi-equilibrium states. We vary the reversion strategies and the preparation of initial states, and observe that the amplitude of the spectra attenuate with the reversion time, and notably, that the decay is frequency selective in all the samples. We interpret this effect as an evidence of “eigen-selection”, a signature of the occurrence of irreversible decoherence, which indicates that the spin system in liquid crystal NMR experiments conforms an actual open quantum system, where quasi-equilibrium can be rigorously described as a stage of the dynamics which develops in a time-scale far earlier than thermal equilibrium. This explanation is supported by a derivation of the observed signals and spectra in terms of the coherences of the spin-system of a single molecule, within the theoretical framework of open quantum systems.

I. INTRODUCTION

The quantum dynamics that drives a quantum system of interacting particles from an initial coherent state into a thermodynamic state are of high concern in physics. The interest relies on fundamental questions as well as on practical applications. Nuclear spins are privileged systems whose quantum dynamics develops in a wide range of time scales that can be accurately probed with Nuclear Magnetic Resonance (NMR). The possibility of preparing different initial quantum states in diverse spin systems, turn them into excellent test-beds for studying the interesting quantum dynamics during their transit from an initial coherent state to the final thermal equilibrium. Particularly, our interest in this work is focused on the intermediate stages, where the irreversible transformation of the initial coherent state into the so called “quasi-equilibrium” (QE) states takes place. Starting from a coherent initial state, QE is attained over a transient period, longer than the time scale characterized by the typical spin interactions. The spin observables associated with this state evolve subsequently only due to spin-lattice relaxation, within a much longer time scale. The mechanism governing the build up of the QE states is still not fully known. It is the aim of this work to provide experimental evidence on its origin.

We consider the spin system formed by the proton spins in liquid crystals (LC). In this kind of sample each molecule constitutes a small cluster of interacting particles, coupled to a highly correlated non-spin environment. In fact, due to the rapid individual molecular motions, the intermolecular spin interactions average out, still, a strong intramolecular residual dipolar energy remains because of the high degree of long range molecular orien-

tation typical of the mesophase [1–3]. The NMR spectroscopic properties of LC are similar to those of solids, that is, the on-resonance free induction decay (FID) signal evolves over a short time scale determined by the local dipolar couplings in the molecule, and the spin-lattice relaxation time scale is much longer than that of the FID. Likewise, it has been shown that in spite of the small number of relevant spin degrees of freedom, the LC spin system can also develop quasi-equilibrium states within a time scale similar to solids [4, 5]. Indeed, the experimental results clearly showed that it is possible to selectively prepare several QE states in LC by adequately setting the preparation pulse sequences [6, 7].

Owing to the small size of the spin system, the attainment of QE in LC cannot be explained through arguments borrowed from statistical mechanics, based on the occurrence of a large number of interacting spins, like spin diffusion. In previous work we anticipated that the development of QE should be related with irreversible adiabatic decoherence [8, 9], that is, with the environment induced decoherence without dissipation. Such a process erodes the off-diagonal elements of the spin density matrix in the “preferred” basis [10], driving the system to a state with a diagonal-in-block form.

We studied the irreversible attenuation of the NMR signals in refocusing experiments (MREV [9] and Magic Echo [11]), and observed that the irreversible decoherence and the development of QE take place within the same characteristic time scale. That is, over an intermediate time scale, considerably earlier than the one dictated by thermal processes. Further theoretical work [8, 9, 11] indicated that a small cluster of interacting spins, viewed as an open quantum system coupled to a correlated environment, can indeed undergo irreversible adiabatic de-

coherence, just as the experimentally observed in LC. A very important feature predicted by this theoretical proposal is that decoherence is controlled by the eigenfrequencies of the spin part of the *interaction* Hamiltonian rather than those of the system Hamiltonian. This phenomenon implies a kind of *selection* (induced by the coupling with the environment) since each element of the density operator decays with a characteristic time, scaled by the corresponding eigenvalue differences, and was accordingly called “eigen-selection” [12]. The occurrence of this effect was experimentally observed on the single-spin single-quantum spectra of some nematic LC [9]. The experiment showed that the higher frequency components of the spectra of the reverted signals attenuate with a higher rate than the lower frequency components, and this behaviour cannot be attributed to experimental non-idealities (non-reverted terms, pulse setting errors, etc).

In this work, we present an NMR experiment designed to display the evolution of coherences during the buildup of a QE state. The technique is applied on several liquid crystals. The experiment aims to visualizing the spectra of the different coherences during the formation of the QE and combines the Jeener-Broekaert (JB) sequence [13] with reversion of the dynamics and encoding of all the coherence orders. This method allows to show the effect of eigen-selection during decoherence, which produces the characteristic frequency compression on the spectra. We are particularly interested on exploring the transient to QE states other than the traditional dipolar order (two-spin order), featured by a higher multi-spin character. We expect to detect the traces of decoherence in the non-equilibrium MQC spectra. An additional convenience of the small-sized spin systems of LC is the possibility of performing the exact numerical calculation of the density operator that would be expected in a closed-system evolution in a small spin cluster. This allows comparison between the calculated and experimental NMR signals. In this way, we bring new evidence which suggests that decoherence in spin systems is produced by the quantum coupling with the environment.

In Section II we explain general aspects of the experiment which tracks the evolution of coherences and spectra during the buildup of quasi-equilibrium states and Section II A contains an analytical description of the signals. The particular case of the output spectra in nematic liquid crystals treated as open quantum systems is described in Section II B. Section III shows the experimental results, and in Section IV we expose the conclusions of the work. Appendix A is added to show the effect of non-idealities on the outcome of the experiment on a hypothetically closed system.

II. DESCRIPTION OF THE PULSE SEQUENCE

The experiment was tailored to study the way in which decoherence affects the frequency content of the spectra of different coherences through eigen-selection [8, 9]

during the transit from a multi-spin initial state to the quasi-equilibrium. The sequence combines the Jeener Broekaert (JB) experiment with encoding of multiple quantum coherences and refocalization of the spin dynamics under the secular dipolar Hamiltonian.

In the standard JB sequence $[(\pi/2)_x - t_p - (\pi/4)_y - t - (\pi/4)_{y+\varphi}]$ (top row in Figure 1(a), with $\tau = 0$), the first $(\pi/2)_x$ pulse produces an initial state of one-spin single quantum coherence which evolves freely under the secular dipolar Hamiltonian during t_p , developing more complex multispin, single-quantum coherences. The second pulse $(\pi/4)_y$ rotates the state into a multi-spin multiple-quantum state (zero, single, double or higher order). The state so prepared is allowed to evolve freely during a waiting time t . If t is “long enough” the spin system reaches a QE state consistent with a diagonal density operator (in the basis of the dipolar Hamiltonian); let us call t_{QE} to the time scale needed for the particular spin system to reach quasi-equilibrium. A last read pulse $(\pi/4)_y$ projects part of the QE state into observable single quantum coherence. The QE state which can be observed after the read pulse depends on the preparation time, in fact, it was shown that at least three different QE states can be observed in nematic liquid crystals [7].

The experiment proposed in this work, depicted in Figure 1(a), aims to make visible the effect of decoherence during the development of quasi-equilibrium, we thus (i) prepare multiple quantum coherences, (ii) display their spectra, and (iii) observe the spectra during their evolution towards quasi-equilibrium. We prepare the initial state with the first phase shifted pair of pulses of the JB sequence and use the phase φ of the read pulse to encode the different coherence orders [14]. The experiment is repeated while incrementing the waiting time t in steps, so that a Fourier Transform on t and φ gives the spectra of each coherence order separately [15]. The important information of the effect of decoherence on the spectra is probed by adding a block, marked as D in Figure 1(a), at the end of which the free evolution under \mathcal{H}_D^0 during time τ has been reverted. The effect of block D is thus to “filter” the reversible evolution. The consequences of the irreversible mechanisms on the signal are then observed by incrementing the duration of block D , as shown in the rows in Figure 1(a).

We use two different schemes for the reversed dynamics to ensure that the results are independent of the particular experimental strategy. Some compounds were studied with the MREV8 sequence [9, 16–18], schematized in Figure 1(b) and other with the ‘magic-sandwich’ (MS) sequence [11, 19–23] (see Figure 1(c)). Each sequence offers particular advantages: MREV can be both used with a continuous variation of the time τ_1 or by concatenating blocks of this sequence [9], so allowing a thorough scan of the decoherence time; MS involves less (although longer) pulses, and is consequently less vulnerable to errors in the pulse settings.

In summary, Figure 1(a) illustrates the whole experiment, where a set of sequences at different refocusing

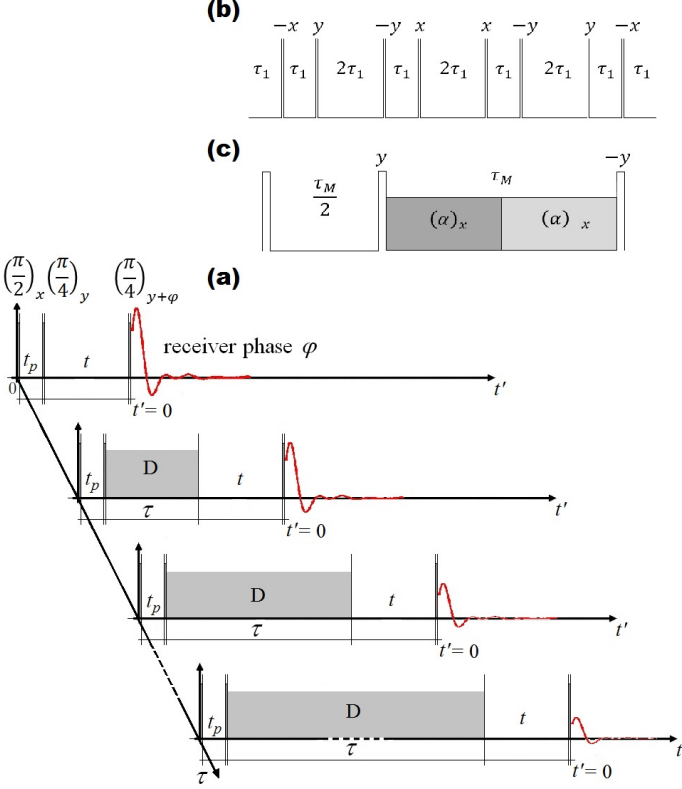


FIG. 1. (a) The pulse sequence used to trace the formation of quasi-equilibrium starts with the phase-shifted pulse pair of the JB sequence, where t_p serves to select the QE state that will develop at the end of the sequence. The waiting time t is incremented in steps as well as the phase φ of the read pulse. Fourier Transformation on t and φ gives the spectra of each coherence order separately. Within block D of duration τ , the system undergoes a reversion dynamics while evolving towards the quasi-equilibrium. The reversion strategies used in the experiment consist of (b): the MREV8 sequence, where $\tau = 12\tau_1$; or (c): the ‘magic-sandwich’ sequence, where $\tau = 1.5\tau_M$

times τ are vertically arranged in order to imitate the bidimensional disposition chosen to show the experimental results (see Section III). Each row represents the set of $N_t \times N_\varphi$ experiments needed to calculate the spectra of all the encoded coherences (where N_t is the number of steps of t and N_φ the number of phase steps in the read pulse). The next sections contain a derivation of the output signals of this experiment and the interpretation of the corresponding spectra in the framework of the theory of open quantum systems.

A. Description of the signals and spectra

When the observed spin system in an NMR experiment is considered as an open quantum system in contact with

an external bath, the total Hamiltonian can be written as

$$\hat{\mathcal{H}} = \hat{\mathcal{H}}_S + \hat{\mathcal{H}}_L + \hat{\mathcal{H}}_{SL}, \quad (1)$$

where the system of interest is described, in isolation, by $\hat{\mathcal{H}}_S$; $\hat{\mathcal{H}}_L$ is the Hamiltonian of the external reservoir and $\hat{\mathcal{H}}_{SL}$ represents the system-bath interaction which has both spin and non-spin variables (e.g. interaction between spins and mechanical variables, or a boson bath, etc.). The hat symbol over operators stands for the “rotating frame” representation: one which rotates around the quantization axis z at the Larmor frequency, and where the spin Hamiltonian $\hat{\mathcal{H}}_S$ does not include the Zeeman term $\mathcal{H}_Z \equiv -\omega_0 \mathbf{I}_z$.

Since we are interested in describing processes which take place in a timescale earlier than relaxation and thermalization effects, the Hamiltonians satisfy the *adiabatic* condition [8, 24, 25]

$$[\hat{\mathcal{H}}_S, \hat{\mathcal{H}}_{SL}] = 0. \quad (2)$$

Assuming adiabaticity is equivalent to excluding energy exchange between the spins and the bath and allows factorizing the total evolution operator as

$$\hat{\mathcal{U}}_T(t) \equiv e^{-i\hat{\mathcal{H}}_S t} e^{-i(\hat{\mathcal{H}}_{SL} + \hat{\mathcal{H}}_L)t} = \hat{\mathcal{U}}(t) \hat{\mathcal{U}}_{SL}(t), \quad (3)$$

where the evolution operator

$$\hat{\mathcal{U}}(t) \equiv e^{-i\hat{\mathcal{H}}_S t} \quad (4)$$

acts on the spin degrees of freedom only and describes the dynamics of a closed system. The “openness” enters in the evolution under the non-commuting terms $\hat{\mathcal{H}}_{SL} + \hat{\mathcal{H}}_L$

$$\hat{\mathcal{U}}_{SL}(t) \equiv e^{-i(\hat{\mathcal{H}}_{SL} + \hat{\mathcal{H}}_L)t}. \quad (5)$$

See Section II 2 from [8] or Section II A from [9] for details about the dynamics under these operators.

The initial equilibrium state of the complete system can be written as the tensor product $\hat{\rho}_{(eq)} = \hat{\rho}_{S(eq)} \rho_{L(eq)}$, where $\hat{\rho}_{S(eq)} \propto \mathbf{I}_z$ represents the spin system in equilibrium with an external field \vec{B}_0 in the high temperature regime, and $\rho_{L(eq)}$ is the density operator of the non-spin degrees of freedom (which is not affected by the RF pulses nor by the evolution under only-spin operators).

The first $(\pi/2)_x$ pulse leaves the spin state as

$$\hat{\rho}_S(0) = \mathbf{R}_x(\pi/2) \mathbf{I}_z \mathbf{R}_x(-\pi/2) = \mathbf{I}_y, \quad (6)$$

where the pulse operator $\mathbf{R}_\alpha(\theta) \equiv e^{i\mathbf{I}_\alpha \theta}$ represents a rotation through an angle θ around the direction α .

After the first pulse, the state evolves under the total evolution operator of Eq. (3). However, it is worth to notice that both the preparation time t_p and the acquisition time t' , used in the experiment outlined in Figure 1, are much shorter (few tens of microseconds) than the timescale scanned by the sum $\tau + t$ (tens to hundreds

of microseconds). Since the dynamics driven by $\hat{\mathbf{U}}_{SL}$ is slower than that driven by $\hat{\mathbf{U}}$, we can consider that

$$\hat{\mathbf{U}}_{SL}(t) \sim \mathbf{1} \text{ during short times } t, \quad (7)$$

which justifies assuming a purely unitary dynamics during t_p and t' . Then, under the assumption (7) the state at the end of the preparation period is $\hat{\rho}(t_p) = \hat{\mathbf{U}}(t_p) \hat{\rho}_S(0) \hat{\mathbf{U}}^\dagger(t_p) \rho_{L(eq)}$. On the contrary, we expect the effect of decoherence due to the inevitable quantum coupling with the environment, to manifest during $\tau + t$.

The second pulse $(\pi/4)_y$ rotates the spin state developed at t_p and transforms it in a spin density operator with terms of zero, single, double or higher order coherence, and the state immediately after preparation is

$$\hat{\rho}(t_p^+) = \mathbf{R}_y(\pi/4) \hat{\rho}_S(t_p) \mathbf{R}_y(-\pi/4) \rho_{L(eq)}. \quad (8)$$

After the second pulse, the state is driven through a forward-backwards evolution during τ , which has the effect of undoing the evolution under the secular dipolar Hamiltonian, but, in principle, cannot undo the evolution under $\hat{\mathcal{H}}_{SL} + \hat{\mathcal{H}}_L$. Let us represent this evolution by the operator $\hat{\mathbf{U}}_R(\tau)$ [26]. Then, the density operator after the reversion period (τ) and the free-evolution (during t) is

$$\hat{\rho}(t, \tau, t_p) = \hat{\mathbf{U}}_T(t) \hat{\mathbf{U}}_R(\tau) \hat{\rho}_S(t_p^+) \rho_{L(eq)} \hat{\mathbf{U}}_R^\dagger(\tau) \hat{\mathbf{U}}_T^\dagger(t). \quad (9)$$

Since this state is no longer separable and we are concerned in calculating the signals produced by the spin observables, we use the spin reduced density matrix defined as

$$\hat{\sigma}(t, \tau, t_p) \equiv \text{tr}_e \{ \hat{\rho}(t, \tau, t_p) \}, \quad (10)$$

where the partial trace $\text{tr}_e \{ \cdot \}$ runs over the environment variables. It is worth to note that $\hat{\sigma}$ as well as $\hat{\rho}_S$ are both density operators which apply only over the spin Hilbert space, but the definition (10) implies that the dynamics that affects to $\hat{\sigma}$ can be non-unitary.

Finally, a read pulse is used to rotate the tensor components with arbitrary ν , into one with $\nu = \pm 1$. The read pulse phase $\pi/2 + \varphi$ (represented as $\mathbf{y} + \varphi$ in the pulse operator) is varied systematically (and consequently the receiver phase) in order to encode the coherence order. Therefore, the NMR signal \mathcal{S} , as a function of the acquisition time t' and the other variable parameters of the experiment (φ, t, τ and t_p), is

$$\mathcal{S}_\alpha(t', \varphi, t, \tau, t_p) = \text{tr} \{ \mathbf{I}_\alpha \hat{\mathbf{U}}(t') \mathbf{R}_{\mathbf{y}+\varphi}(\pi/4) \times \hat{\sigma}(t, \tau, t_p) \mathbf{R}_{\mathbf{y}+\varphi}(-\pi/4) \hat{\mathbf{U}}^\dagger(t') \}, \quad (11)$$

where $\alpha = \mathbf{x}$ or \mathbf{y} . In Eq. (11) we also used the approximation (7) because we only need the signal at the earliest acquisition times t' . Using that

$$\mathbf{R}_{\mathbf{y}+\varphi}(\pi/4) = \mathbf{R}_z(-\varphi) \mathbf{R}_y(\pi/4) \mathbf{R}_z(\varphi), \quad (12a)$$

$$\mathbf{I}_{(\mathbf{x}, \mathbf{y})+\varphi} = \mathbf{R}_z(-\varphi) \mathbf{I}_{(\mathbf{x}, \mathbf{y})} \mathbf{R}_z(\varphi), \quad (12b)$$

and after some algebra, the signal can be written as

$$\mathcal{S}_\alpha = \text{tr} \{ \mathbf{I}_\alpha \hat{\mathbf{U}}(t') \mathbf{R}_y(\pi/4) \mathbf{R}_z(\varphi) \hat{\sigma}(t, \tau, t_p) \times \mathbf{R}_z(-\varphi) \mathbf{R}_y(-\pi/4) \hat{\mathbf{U}}^\dagger(t') \}. \quad (13)$$

In order to disclose the coherence encoding implicit in Eq. (13), it is useful to write the reduced density operator in terms of a set of irreducible tensors $\{ \mathbf{T}_{\lambda\nu}^\Lambda \}$ which serve as an operator basis for the Liouville space where $\hat{\sigma}$ belongs. Index λ is the tensor rank, ν the component number, and Λ distinguishes between different species of tensors with the same rank [27]. The reduced density operator at any time is formally

$$\hat{\sigma}(t, \tau, t_p) = \sum_\Lambda \sum_{\lambda\nu} \xi_{\lambda\nu}^\Lambda(t, \tau, t_p) \mathbf{T}_{\lambda\nu}^\Lambda. \quad (14)$$

where

$$\xi_{\lambda\nu}^\Lambda(t, \tau, t_p) = \text{tr} \{ \mathbf{T}_{\lambda\nu}^\Lambda \hat{\sigma}(t, \tau, t_p) \} \quad (15)$$

is the projection of $\hat{\sigma}(t)$ on $\mathbf{T}_{\lambda\nu}^\Lambda$, which satisfies

$$\text{tr} \{ \mathbf{T}_{\lambda\nu}^\Lambda \mathbf{T}_{\lambda'\nu'}^{\Lambda'} \} = \delta_{\Lambda, \Lambda'} \delta_{\lambda, \lambda'} \delta_{\nu, \nu'} \equiv \delta_{\Lambda' \lambda' \nu'}^{\Lambda \lambda \nu},$$

and δ is the Kronecker delta.

Finally, using expansion (14) in Eq. (13), and the fact that

$$\mathbf{R}_z(\varphi) \mathbf{T}_{\lambda\nu}^\Lambda \mathbf{R}_z(-\varphi) = e^{i\nu\varphi} \mathbf{T}_{\lambda\nu}^\Lambda, \quad (16)$$

the NMR signals measured under the sequences of Figure 1 can be expressed as

$$\mathcal{S}_\alpha(t', \varphi, t, \tau, t_p) = \sum_\nu e^{i\nu\varphi} \sum_{\Lambda\lambda} g_{\lambda\nu}^{\Lambda, \alpha}(t') \xi_{\lambda\nu}^\Lambda(t, \tau, t_p), \quad (17)$$

where

$$g_{\lambda\nu}^{\Lambda, \alpha}(t') \equiv \text{tr} \{ \mathbf{I}_\alpha \hat{\mathbf{U}}(t') \mathbf{R}_y(\pi/4) \mathbf{T}_{\lambda\nu}^\Lambda \mathbf{R}_y(-\pi/4) \hat{\mathbf{U}}^\dagger(t') \}. \quad (18)$$

In our experiment, instead of $g_{\lambda\nu}^{\Lambda, \alpha}(t')$ we used $g_{\lambda\nu}^{\Lambda, \alpha}(t'_m)$, the average value of the signals within an interval Δ centered at the earliest measuring time $t' \equiv t'_m$ where the signal has its maximum absolute value in some experimental outcome. That is

$$g_{\lambda\nu}^{\Lambda, \alpha}(t'_m) \equiv \frac{1}{\Delta} \int_{t'_m - \Delta/2}^{t'_m + \Delta/2} g_{\lambda\nu}^{\Lambda, \alpha}(t') dt', \quad (19)$$

The spectra of coherences emerge after calculating the Fourier transform of Eq. (17) over the variables t and φ , that is

$$\mathcal{F}_{\varphi, t} \{ \mathcal{S} \} (t'_m, \mu, \omega, \tau, t_p) = \sum_\nu \delta(\mu - \nu) \sum_{\Lambda\lambda} g_{\lambda\nu}^{\Lambda, \alpha}(t'_m) \mathcal{F}_t \{ \xi_{\lambda\nu}^\Lambda \} (\omega, \tau, t_p), \quad (20)$$

where $\mathcal{F}_\alpha \{f(\alpha)\}(\beta)$ represents the Fourier transform of function f over the variable α , and β is the conjugate variable of α . In Eq. (20), μ and ω are the conjugate variables of φ and t , respectively.

Equation (20) stands for the coherence spectra obtained at a given combination of preparation time t_p and evolution under reverse dynamics in τ . The novelty it introduces comes in the non-unitary dynamics along the intermediate time scale τ , which enters in the observed spectra through the Fourier transform of the coefficient $\xi(t, \tau, t_p)$. If the observed system were actually closed, its NMR signal would not depend on τ because the dynamics would be completely reversible. However such a reversible behaviour could be a fictitious expectation since actual physical systems are not closed, indeed, the subtle quantum correlation between the observed system and its environment (even without energy exchange) may cause decoherence [8, 9]. Thus, any observed τ dependence might be interpreted either as an indication of an irreversible (non-unitary) behaviour, or as the result of an incorrect experimental setting.

In the next section, we write (20) for the case of nematic liquid crystals (NLC), where the *eigen-selection* effect on the spectra of the coherences under reversion dynamics, becomes evident [8, 9].

B. The case of nematic liquid crystals

This section is dedicated to obtain an analytical expression of the output signals of the experiment of Section II on a NLC sample, considered as an open quantum system. We first analyze the reasonable assumption that in a state prepared at t_p there is no particular correlation among the spin variables of different LC molecules. However, the subsequent evolution under $\hat{U}_T(t)$ and $\hat{U}_R(\tau)$ may mix the Hilbert spaces of different molecules and turn the state into a correlated one. Then, in order to facilitate the analysis of the experiment in terms of the characteristic features of the nematic ordering, in Section IIB2 we write the state at the end of the pulse sequence described above in terms of the state of a single molecule.

1. Initial non-correlated condition

The main contribution to the total spin Hamiltonian in NLC comes from the dipole-dipole interaction. The fast molecular diffusion occurring in the nematic state, averages out the inter-molecular dipolar interaction, leaving only the intra-molecular part [2]. This characteristic of orientationally ordered phases allows writing the spin Hamiltonian $\hat{\mathcal{H}}_S$ of a NLC in a separable form [8, 9], in terms of the single molecule Hamiltonians

$$\hat{\mathcal{H}}_S \equiv \sum_i \hat{\mathcal{H}}_{S_i}^{(s)} \otimes \mathbf{1}^{(e)}, \quad (21)$$

with $\hat{\mathcal{H}}_{S_i}^{(s)} \equiv \mathbf{1}^{(s_1)} \otimes \dots \otimes \hat{\mathcal{H}}_S^{(s_i)} \otimes \dots \otimes \mathbf{1}^{(s_N)}$, where the superscripts between parentheses indicate different Hilbert spaces: (s) for the whole spin sample, (s_i) for the spins that belong to the i -th molecule and (e) for the environment, non-spin variables. $\hat{\mathcal{H}}_S^{(s_i)}$ is the secular dipolar Hamiltonian of a single molecule, in the high-field approximation

$$\hat{\mathcal{H}}_S^{(s_i)} \equiv \frac{1}{2} S_{zz} \sum_{j \neq k}^{(i)} \sqrt{\frac{2}{3}} \omega_D(r_{ij}) \mathbf{T}_{20}^{jk(s_i)}. \quad (22)$$

The symbol $\sum^{(i)}$ in Eq. (22) represents a sum that runs over the sites of the resonant nuclei within the i -th molecule, and $\mathbf{T}_{20}^{jk(s_i)}$ is the secular irreducible spherical tensor of second rank which applies over the Hilbert space of the i -th molecule,

$$\mathbf{T}_{20}^{jk(s_i)} \equiv \frac{1}{\sqrt{6}} \left[2 \mathbf{I}_{zj} \mathbf{I}_{zk} - \frac{1}{2} (\mathbf{I}_{+j} \mathbf{I}_{-k} + \mathbf{I}_{-j} \mathbf{I}_{+k}) \right]^{(s_i)}, \quad (23)$$

where $\mathbf{I}_{\alpha k}$ is the α -component of the angular momentum of the k -th spin and $[\cdot]^{(s_i)}$ indicates that the operators apply exclusively over the Hilbert space of the i -th molecule. The dipolar frequency defined in Hz units is

$$\omega_D(r_{kj}) \equiv 3 \frac{\mu_0 \gamma^2 \hbar}{8 \pi r_{kj}^3} [1 - 3 \cos^2(\beta_{jk})], \quad (24)$$

with β_{jk} the polar angle of vector \vec{r}_{jk} joining spins j and k , with respect to the $\hat{\mathbf{z}}$ -axis of the system fixed to the molecule and S_{zz} is the mean value of the molecular order parameter [8], defined as

$$S_{zz} \equiv \left\langle \frac{3}{2} \cos^2 \theta - \frac{1}{2} \right\rangle, \quad (25)$$

with θ the polar angle between the molecular $\hat{\mathbf{z}}$ -axis and the static strong magnetic field \vec{B}_0 .

A consequence of the separability of Hamiltonian (21) is that the inter-molecular correlation is not involved in the Liouvillian evolution, within the adiabatic time scale. Consequently, the evolution operator (4) can be factorized as

$$\hat{U}(t) \equiv \otimes_i e^{-i \hat{\mathcal{H}}_S^{(s_i)} t}, \quad (26)$$

with $\otimes_i \mathbf{O}^{(s_i)} \equiv \mathbf{O}^{(s_1)} \otimes \dots \otimes \mathbf{O}^{(s_i)} \otimes \dots \otimes \mathbf{O}^{(s_N)}$, where it is clear that $\hat{U}(t)$ acts on the spin space of each molecule without mixing their Hilbert spaces.

Let us now consider that the experiment starts from thermal equilibrium. Therefore, the spin part of the density operator is

$$\hat{\rho}_{S(eq)}^{(s)} \equiv \frac{e^{\beta_T \omega_0 \mathbf{I}_z^{(s)}}}{\mathcal{N}_{S_1}^N} \simeq \frac{\mathbf{1}^{(s)}}{\mathcal{N}_{S_1}^N} + \frac{1}{\mathcal{N}_{S_1}^{N-1}} \sum_i \hat{\rho}_{S_i(eq)}^{(s)}, \quad (27)$$

where $\hat{\rho}_{S_i(eq)}^{(s)} \equiv \mathbf{1}^{(s_1)} \otimes \dots \otimes \hat{\rho}_{(eq)}^{(s_i)} \otimes \dots \otimes \mathbf{1}^{(s_N)}$ and $\mathcal{N}_{S_1} \equiv \text{tr}_{s_1} \{ \mathbf{1}^{(s_1)} \}$ is the trace of the identity operator

over the Hilbert space of spins belonging to only one molecule, N is the number of molecules, and we define the equilibrium density operator of the single molecules

$$\hat{\rho}_{(eq)}^{(s_i)} \equiv \frac{\beta_T \omega_0}{\mathcal{N}_{S_1}} \mathbf{I}_{\mathbf{z}}^{(s_i)}, \quad (28)$$

with $\beta_T \equiv \frac{\hbar}{k_B T}$, k_B the Boltzmann constant and T the absolute temperature. The complete thermal equilibrium density matrix, that involves spin and environment variables, is

$$\hat{\rho}_{(eq)} = \hat{\rho}_{S(eq)}^{(s)} \otimes \rho_{L(eq)}^{(e)}. \quad (29)$$

In this way, using Eq. (26) and the initial thermal state (27), the spin density operator from Eq. (8) immediately after the preparation period, for a NLC can be written as

$$\hat{\rho}_S^{(s)}(t_p^+) = \frac{1}{\mathcal{N}_{S_1}^{N-1}} \sum_i \hat{\rho}_{Si}^{(s)}(t_p^+), \quad (30)$$

where $\hat{\rho}_{Si}^{(s)}(t_p^+) = \mathbf{1}^{(s_1)} \otimes \dots \otimes \hat{\rho}^{(s_i)}(t_p^+) \otimes \dots \otimes \mathbf{1}^{(s_N)}$ and

$$\hat{\rho}^{(s_i)}(t_p^+) = \frac{\beta_T \omega_0}{\mathcal{N}_{S_1}} \left[\mathbf{R}_y(\pi/4) \hat{\mathbf{U}}(t_p) \mathbf{I}_y \times \hat{\mathbf{U}}^\dagger(t_p) \mathbf{R}_y(-\pi/4) \right]^{(s_i)}. \quad (31)$$

It should be mentioned that we leave out the identity operator in Eq. (30) because it does not contribute to the NMR signals.

Therefore, the complete density matrix for the state is

$$\hat{\rho}(t_p^+) = \hat{\rho}_S^{(s)}(t_p^+) \otimes \rho_{L(eq)}^{(e)}. \quad (32)$$

In obtaining Eq. (32) (and thus in Eq. (30) as well), we used the approximation (7) and Eq. (8).

Finally, Eq. (32) is the non-correlated initial state whose dynamics under decoherence we calculate in the next section.

2. Evolution of the spectra in an open quantum spin system

We now calculate the dynamics under decoherence in the same way as in Eq. (9), starting from a non-correlated initial state like (32). In this work we will use the expressions for the evolution operators obtained from reference [9], which describe the non-unitary dynamics of a NLC sample[28].

In order to visualize the coherence content of the observable signal as in Eq. (17) and (20), we follow the reasoning which goes from Eq. (9), defines the reduced density operator (10) and spans it on the tensor basis of Eq. (14). It is worth to have in mind that within the time scale where coherences may grow and attenuate, the evolution operator (3) introduces correlations

between the spin Hilbert spaces of different molecules by means of the non-spin or environment variables. Therefore, the reduced density operator (which by definition applies exclusively over the spin space), cannot in principle be written as a linear superposition of tensors acting independently over each molecule. However, we can define a tensor basis for the complete spin Hilbert space as the tensor product of the elements of the single-molecule bases, $\{\otimes_i \mathbf{T}_{\lambda_i \nu_i}^{\Lambda_i(s_i)}\}$. In this way, we can write the expansion of the reduced density operator at any time t as

$$\hat{\sigma}^{(s)}(t, \tau, t_p) = \sum_{\Lambda_1 \lambda_1 \nu_1} \dots \sum_{\Lambda_i \lambda_i \nu_i} \dots \sum_{\Lambda_N \lambda_N \nu_N} \xi_{\{\lambda_i \nu_i\}}^{\{\Lambda_i\}}(t, \tau, t_p) \left[\otimes_i \mathbf{T}_{\lambda_i \nu_i}^{\Lambda_i(s_i)} \right], \quad (33)$$

with

$$\begin{aligned} \xi_{\{\lambda_i \nu_i\}}^{\{\Lambda_i\}}(t, \tau, t_p) &\equiv \text{tr}_s \left\{ \left[\otimes_i \mathbf{T}_{\lambda_i \nu_i}^{\Lambda_i(s_i)} \right] \hat{\sigma}^{(s)}(t, \tau, t_p) \right\} \\ &= \sum_{\zeta s, \zeta' s'} \langle \zeta' s' | \otimes_i \mathbf{T}_{\lambda_i \nu_i}^{\Lambda_i(s_i)} | \zeta s \rangle \langle \zeta s | \hat{\sigma}^{(s)}(t, \tau, t_p) | \zeta' s' \rangle, \end{aligned} \quad (34)$$

where the trace runs over the total spin space. In Eq. (34) the indices in curly brackets indicate dependence on the set of eigenvalues of each molecule of the whole sample, denoted as $\{\Lambda_i\} \equiv \{\Lambda_1, \dots, \Lambda_i, \dots, \Lambda_N\}$ and $\{\lambda_i \nu_i\} \equiv \{\lambda_1 \nu_1, \dots, \lambda_i \nu_i, \dots, \lambda_N \nu_N\}$. Besides, we have the following orthonormality condition

$$\text{tr}_{s_i} \left\{ \mathbf{T}_{\lambda_i \nu_i}^{\Lambda_i(s_i)} \mathbf{T}_{\lambda'_i \nu'_i}^{\Lambda'_i(s_i)} \right\} = \delta_{\Lambda_i, \Lambda'_i} \delta_{\lambda_i, \lambda'_i} \delta_{\nu_i, \nu'_i} \equiv \delta_{\Lambda'_i \lambda'_i \nu'_i}^{\Lambda_i \lambda_i \nu_i}, \quad (35)$$

with $\mathbf{T}_{0,0}^{0(s_i)} \equiv \mathbf{1}^{(s_i)} / \sqrt{\mathcal{N}_{S_1}}$ and $\text{tr}_{s_i} \{\mathbf{T}_{\lambda_i \nu_i}^{\Lambda_i(s_i)}\} = 0$.

In order to calculate the trace in Eq. (34), we use a product basis of the common eigenstates of the spin Hamiltonian, $\hat{\mathcal{H}}_S$, and the spin part of the spin-lattice Hamiltonian [8, 9] of each molecule (remember that the commutation relationship (2) implies the existence of a common eigenbasis), that is

$$\{|\zeta s\rangle \equiv \otimes_i |\zeta_i s_i\rangle\},$$

where ζ_i are the eigenvalues, s_i accounts for the degeneration of each eigenvalue and the eigenstates satisfy $\hat{\mathcal{H}}_S^{(s_i)} |\zeta_i s_i\rangle = S_{zz} \zeta_i |\zeta_i s_i\rangle$.

The elements of the reduced density matrix of Eq. (34) are

$$\begin{aligned} \langle \zeta s | \hat{\sigma}^{(s)}(t, \tau, t_p) | \zeta' s' \rangle &= \langle \zeta s | \text{tr}_e \left\{ \hat{\rho}^{(s)}(t, \tau, t_p) \right\} | \zeta' s' \rangle \\ &= \sum_i \frac{e^{-i(\zeta_i - \zeta'_i) S_{zz} t}}{\mathcal{N}_{S_1}^{N-1}} \langle \zeta_i s_i | \hat{\rho}^{(s_i)}(t_p^+) | \zeta'_i s'_i \rangle \\ &\quad \times \prod_{j \neq i} \delta_{\zeta'_j s'_j}^{\zeta_j s_j} G_{\{\zeta, \zeta'\}}(t, \tau). \end{aligned} \quad (36)$$

where $G_{\{\zeta, \zeta'\}}(t, \tau)$ is the decoherence function associated with the non-unitary evolution due to the spin-environment coupling. This function is defined from the general expression

$$G_{\{\zeta, \zeta'\}}(t, \tau) = \text{tr}_e \left\{ \hat{\mathbf{U}}^{(e)\dagger}(\zeta', t, \tau) \hat{\mathbf{U}}^{(e)}(\zeta, t, \tau) \rho_{L(eq)}^{(e)} \right\}, \quad (37)$$

where the indices ζ and ζ' represent the set of eigenvalues of all the molecules, that is $\zeta \equiv \{\zeta_1, \dots, \zeta_i, \dots, \zeta_N\}$ and $\zeta' \equiv \{\zeta'_1, \dots, \zeta'_i, \dots, \zeta'_N\}$. The evolution operator $\hat{\mathbf{U}}^{(e)}(\zeta, t, \tau)$ acts on the environment degrees of freedom only, and is defined from the evolution operators $\hat{\mathbf{U}}_T(t)$ and $\hat{\mathbf{U}}_R(\tau)$ (which apply over the spin and the environment Hilbert space) as follows

$$\hat{\mathbf{U}}^{(e)}(\zeta, t, \tau) \equiv \langle \zeta_s | e^{i \hat{\mathcal{H}}_s^{(s)} t} | \zeta_s \rangle \langle \zeta_s | \hat{\mathbf{U}}_T(t) \hat{\mathbf{U}}_R(\tau) | \zeta_s \rangle. \quad (38)$$

In this way, the decoherence function in Eq. (36) is obtained by applying the condition $\zeta_j = \zeta'_j, \forall j/j \neq i$ on Eq. (37). Therefore, $G_{\{\zeta, \zeta'\}}$ depends on all the values $\zeta_1, \dots, \zeta_i, \dots, \zeta_N$ and on ζ'_i . Further properties of the decoherence function are explained in reference [9]. The product symbol used in Eq. (36) stands for the product of the $N - 1$ Kronecker deltas of all the molecules except the one with $j = i$, that is

$$\prod_{j \neq i} \delta_{\zeta'_j s'_j}^{\zeta_j s_j} \equiv \delta_{\zeta_1 s_1, \zeta'_1 s'_1} \cdots \delta_{\zeta_N s_N, \zeta'_N s'_N}.$$

Using Eq. (36) in Eq. (34), and after of some manipulation with the ordering of indices, we obtain

$$\begin{aligned} \xi_{\{\lambda_i \nu_i\}}^{\{\Lambda_i\}}(t, \tau, t_p) &= \sum_i \sum_{\zeta_i s_i, \zeta'_i s'_i} e^{-i(\zeta_i - \zeta'_i) S_{zz} t} \\ &\times \langle \zeta_i s_i | \hat{\rho}^{(s_i)}(t_p^+) | \zeta'_i s'_i \rangle \langle \zeta'_i s'_i | \mathbf{T}_{\lambda_i \nu_i}^{\dagger \Lambda_i(s_i)} | \zeta_i s_i \rangle \frac{1}{\mathcal{N}_{S_1}^{N-1}} \\ &\times \sum_{\zeta_k \neq \zeta_i, s_k \neq s_i} \left[\prod_{j \neq i} \langle \zeta_j s_j | \mathbf{T}_{\lambda_j \nu_j}^{\dagger \Lambda_j(s_j)} | \zeta_j s_j \rangle \right] G_{\{\zeta, \zeta'\}}(t, \tau), \end{aligned} \quad (39)$$

where the sum $\sum_{\zeta_k \neq \zeta_i, s_k \neq s_i}$ runs over the values of $\zeta_k s_k$ different from $\zeta_i s_i$. Besides, the sum affects the factors in the product and the decoherence function as well [29].

The coefficient (39) introduces the effects of decoherence in the dynamics of the density matrix (33), through the decay function $G_{\{\zeta, \zeta'\}}(t, \tau)$. It is important to remark that this decoherence function emerges in the spin density operator as a consequence of recognizing the coupling with the environment and involving it into the spin dynamics.

It is worth to note that, in principle, the decoherence function introduces quantum correlations between the molecules of the NLC, even when there is no direct interaction between spins belonging to different molecules. In order to get insight on the significance of the decoherence

function and also to exhibit its relation with the observed signals and spectra, we first assume the existence of different time scales for different mechanism of decoherence. As can be seen from Section II B of reference [9], the decoherence factors that affect to the i -th molecule and that depend on the eigenvalues ζ_j (with $j \neq i$) of the rest of the molecules have slower decay than that produced by the reversible AQD (which depends on the eigenvalue ζ_i only), thus they can be neglected in front of the reversible decoherence factor. Therefore, the decoherence function depend on the spin variables of each molecule only, that is,

$$G_{\{\zeta, \zeta'\}}(t, \tau) \cong G_{\{\zeta_i, \zeta'_i\}}(t, \tau). \quad (40)$$

We also make the following plausible assumptions (called **HypoG-I** and **HypoG-II** in Ref. [9]). One is the *statistical independence between the eigenvalues* of the spin-bath interaction of each molecule and the eigenvalues of commutators of such Hamiltonians, which allows to separate the decoherence function in two factors

$$G_{\{\zeta_i, \zeta'_i\}}(t, \tau) \equiv G_{\{\zeta_i, \zeta'_i\}}^T(t) G_{\{\zeta_i, \zeta'_i\}}^R(\tau). \quad (41)$$

The first factor represents the *strictly adiabatic quantum decoherence* (AQD) [8], which is responsible for the line-shape of the coherence spectra and is the main decoherence process in a free evolution dynamics. It takes place in a time scale shorter than the rest of the decoherence processes and its dynamics is in principle reversible. The second factor accounts for the *essentially adiabatic quantum decoherence* [8], it is of irreversible character and has a slower dynamics than the reversible AQD. The second hypothesis is to consider an *homogeneous environment for each molecule*, i.e. *absence of border effects*, where each molecule sees the same neighborhood, which implies that the function is the same for each molecule, this is $G_{\{\zeta_i, \zeta'_i\}}(t, \tau) = G_{\{\zeta_j, \zeta'_j\}}(t, \tau) \forall i, j$.

In order to simplify the coefficient (39), we see that assumption (40) implies that the decoherence function in the sum only depends on the spin variables ζ_i and ζ'_i of the i -th molecule, and thus can be extracted out of the sum $\sum_{\zeta_k \neq \zeta_i, s_k \neq s_i}$ which excludes the i -th molecule. We thus denote the resulting sum as

$$\begin{aligned} \mathcal{A}_{j \neq i}^{\{\Lambda_j \lambda_j \nu_j\}} &\equiv \sum_{\zeta_k \neq \zeta_i, s_k \neq s_i} \left[\prod_{j \neq i} \langle \zeta_j s_j | \mathbf{T}_{\lambda_j \nu_j}^{\dagger \Lambda_j(s_j)} | \zeta_j s_j \rangle \right] / \mathcal{N}_{S_1}^{N-1} \\ &= \prod_{j \neq i} \text{tr}_{s_j} \{ \mathbf{T}_{\lambda_j \nu_j}^{\dagger \Lambda_j(s_j)} \} / \mathcal{N}_{S_1}^{N-1}. \end{aligned} \quad (42)$$

Because of the orthogonal property (35) and the fact that the identity operator forms part of the tensor basis,

the rest of the basis operators have null trace. Therefore,

$$\mathcal{A}_{j \neq i}^{\{\Lambda_j, \lambda_j, \nu_j\}} = \begin{cases} \frac{1}{\mathcal{N}_{S_1}^{N-1}} \prod_{j \neq i} tr_{s_j} \left\{ \frac{\mathbf{1}^{(s_j)}}{\sqrt{\mathcal{N}_{S_1}^{N-1}}} \right\} = \frac{1}{\sqrt{\mathcal{N}_{S_1}^{N-1}}} \\ \text{(If } \forall j \Lambda_j = 0, \lambda_j = 0 \text{ and } \nu_j = 0) \\ 0 \text{ (otherwise)} \end{cases}$$

$$= \prod_{j \neq i} \delta_{\Lambda_j, \lambda_j, \nu_j}^{0,0,0} / \sqrt{\mathcal{N}_{S_1}^{N-1}}, \quad (43)$$

where $\delta_{\Lambda_j, \lambda_j, \nu_j}^{0,0,0} \equiv \delta_{\Lambda_j, 0} \delta_{\lambda_j, 0} \delta_{\nu_j, 0}$.

Finally, the commented considerations over the decoherence function together with (43) in Eq. (39), allow writing

$$\xi_{\{\lambda_i \nu_i\}}^{\{\Lambda_i\}}(t, \tau, t_p) = \sum_i \xi_{\lambda_i \nu_i}^{\Lambda_i}(t, \tau, t_p) \prod_{j \neq i} \delta_{\Lambda_j, \lambda_j, \nu_j}^{0,0,0} / \sqrt{\mathcal{N}_{S_1}^{N-1}}, \quad (44)$$

where

$$\xi_{\lambda_i \nu_i}^{\Lambda_i}(t, \tau, t_p) \equiv \sum_{\zeta_i s_i, \zeta'_i s'_i} e^{-i(\zeta_i - \zeta'_i) S_{zz} t} G_{\{\zeta_i, \zeta'_i\}}^T(t) G_{\{\zeta_i, \zeta'_i\}}^R(\tau) \times \langle \zeta_i s_i | \hat{\rho}^{(s_i)}(t_p^+) | \zeta'_i s'_i \rangle \langle \zeta'_i s'_i | \mathbf{T}_{\lambda_i \nu_i}^{\Lambda_i(s_i)} | \zeta_i s_i \rangle, \quad (45)$$

which only depends on the coefficients Λ_i , λ_i and ν_i of the i -th molecule, with $\xi_{\lambda_i \nu_i}^{\Lambda_i}(t, \tau, t_p) = \xi_{\lambda_j \nu_j}^{\Lambda_j}(t, \tau, t_p)$, $\forall i, j$.

Let us now go back to the spin reduced density matrix of Eq. (33) and replacing the coefficient (44) we get a factorized form

$$\hat{\sigma}^{(s)}(t, \tau, t_p) = \sum_i \frac{\mathbf{1}^{(s_1)}}{\mathcal{N}_{S_1}} \otimes \dots \otimes \hat{\sigma}^{(s_i)}(t, \tau, t_p) \otimes \dots \otimes \frac{\mathbf{1}^{(s_N)}}{\mathcal{N}_{S_1}}, \quad (46)$$

where each factor $\hat{\sigma}^{(s_i)}(t, \tau, t_p)$ corresponds to a single molecule, and also satisfies $\hat{\sigma}^{(s_i)}(t, \tau, t_p) = \hat{\sigma}^{(s_j)}(t, \tau, t_p) \forall i, j$.

It is worth to note that the product of Kronecker delta functions that arise on Eq. (44), make the expansion (33) to adopt a non-correlated form in the spin variables, that is, the sum over the indices λ_i, ν_i and Λ_i of the i -th molecule involve tensor operators which apply on the Hilbert space of such molecule (with identities on the indices of the other molecules). We could then describe the time dependence of the reduced density operator of Eq. (44) in terms of single-molecule decoherence functions which however enclose quantum *inter-molecular* correlations. That is, there is no direct spin interaction between different molecules but they become correlated because of the more subtle quantum interplay between $\hat{\mathcal{H}}_S$ and $\hat{\mathcal{H}}_{SL}$

As a final step, we use the density operator (46) in

Eq. (13) to calculate the expression for the signal (17)

$$\mathcal{S}_\alpha(t', \varphi, t, \tau, t_p) = N \sum_{\nu_1} e^{i\nu_1 \varphi} \sum_{\Lambda_1 \lambda_1} g_{\lambda_1 \nu_1}^{\Lambda_1, \alpha}(t') \xi_{\lambda_1 \nu_1}^{\Lambda_1}(t, \tau, t_p), \quad (47)$$

where, similarly to Eq. (18),

$$g_{\lambda_1 \nu_1}^{\Lambda_1, \alpha}(t') \equiv tr_{s_1} \left\{ \left[\mathbf{I}_\alpha \hat{\mathbf{U}}(t') \mathbf{R}_Y(\pi/4) \mathbf{T}_{\lambda_1 \nu_1}^{\Lambda_1} \times \mathbf{R}_Y(-\pi/4) \hat{\mathbf{U}}^\dagger(t') \right]^{s_1} \right\}. \quad (48)$$

Equation (47) shows that the signal generated by the total sample of a NCL is N times the signal generated by one molecule (here labelled as molecule 1), with N the total number of molecule in the sample.

Finally, the evolution of the spectra for a NLC, measured by means of the experiment shown in Figure 1 is

$$\mathcal{F}_{\varphi, t} \{ \mathcal{S} \} (t'_m, \mu, \omega, \tau, t_p) = N \sum_{\nu_1} \delta(\mu - \nu_1) \sum_{\Lambda_1 \lambda_1} g_{\lambda_1 \nu_1}^{\Lambda_1, \alpha}(t'_m) \mathcal{F}_t \left\{ \xi_{\lambda_1 \nu_1}^{\Lambda_1} \right\} (\omega, \tau, t_p), \quad (49)$$

with $g_{\lambda_1 \nu_1}^{\Lambda_1, \alpha}(t'_m)$ defined as in Eq. (19). Besides, using Eq. (45) in Eq. (49), the Fourier transform in t can be written as

$$\mathcal{F}_t \left\{ \xi_{\lambda_1 \nu_1}^{\Lambda_1} \right\} (\omega, \tau, t_p) = \sum_{\zeta_1 s_1, \zeta'_1 s'_1} G_{\{\zeta_1, \zeta'_1\}}^R(\tau) \times \frac{2\pi}{|\zeta'_1 - \zeta_1|} p \left(\frac{\omega - (\zeta'_1 - \zeta_1) S_{zz}}{\zeta'_1 - \zeta_1} \right) \times \langle \zeta_1 s_1 | \hat{\rho}^{(s_1)}(t_p^+) | \zeta'_1 s'_1 \rangle \langle \zeta'_1 s'_1 | \mathbf{T}_{\lambda_1 \nu_1}^{\Lambda_1(s_1)} | \zeta_1 s_1 \rangle, \quad (50)$$

where we use the result

$$\mathcal{F}_t \left\{ e^{-i(\zeta_1 - \zeta'_1) S_{zz} t} G_{\{\zeta_1, \zeta'_1\}}^T(t) \right\} = \frac{2\pi}{|\zeta'_1 - \zeta_1|} p \left(\frac{\omega - (\zeta'_1 - \zeta_1) S_{zz}}{\zeta'_1 - \zeta_1} \right), \quad (51)$$

which was calculated in Section II B of reference [9]. In (50) the function p is the called orientational molecular distribution function (OMDF) [8], which is the Fourier transform of the reversible AQD function.

To conclude this section, we can observe from (49), (50) and (51) the following properties: The reversible AQD gives rise to the line-shape of every coherence, as comes out from Eqs.(49) and (50). Such spectra are obtained as a superposition of copies of the OMDF shifted to the frequencies $(\zeta'_1 - \zeta_1) S_{zz}$ and scaled by the factor $|\zeta'_1 - \zeta_1|$, as can be seen in (51). The consequence of this scaling is the *eigen-selection* effect in the time domain of t , due to which the larger the value of $|\zeta'_1 - \zeta_1|$, the faster the decay. This is reflected in the spectra making

that for higher frequencies $(\zeta'_1 - \zeta_1)S_{zz}$ the corresponding copy of the OMDF is less intense and wider, which produces a resulting effect of narrowing or compression of the complete spectrum.

On the other hand, the irreversible decoherence function $G_{\{\zeta_1, \zeta'_1\}}^R(\tau)$ has a decay time which depends on the difference of the eigenvalues $\zeta'_1 - \zeta_1$ as well (as an example from reference [9], $G_{\zeta_1, \zeta'_1}^R(\tau) = e^{-(\zeta_1 - \zeta'_1)^2 \sigma_{CL}^2 \tau^4 / [8(\kappa+1)^2]}$), which introduces an alteration of the line-shape as a function of the time τ . Specifically, the frequency distribution of each coherence spectrum (Fourier transform on t) changes with the reversion time: higher frequency components decay faster. This distinctive behaviour, called *eigen-selectivity* [9], is the fingerprint of decoherence associated with an open quantum spin system.

III. EXPERIMENTAL SETUP AND RESULTS

In this section we present the experimental results on liquid crystal samples in the nematic phase, obtained with the pulse sequences shown in Figure 1, and described in Section II.

The experiments which use the reversion sequence MREV8 were carried out on samples of 5CB (4'-pentyl-4-biphenyl-carbonitrile) and PAA₆ (methyl deuterated p-azoxyanisole), using a home-built pulsed spectrometer, based on a Varian EM360 magnet (60MHz for protons). The electronic setup allows control of the pulse phases, homogeneity of the magnetic field, and sample temperature with stability of $\pm 0.1^\circ\text{C}$. Experiments which use the reversion sequence MS were conducted on a Bruker minispec mq20 (20 MHz) on 8CB (4'-octyl-4-biphenyl-carbonitrile).

The experiment starts by setting the time t_p needed to prepare the initial state $\rho_S(t_p^+)$ so that a subsequent free evolution drives the system to the so called “strong” (\mathcal{S} -order) or “weak” \mathcal{W} -order [7]. We test the experiment by preparing the initial state in 5CB with $t_p = 27\mu\text{s}$, since it has already been shown that after a transient $t \sim 1\text{ms}$ the system reaches the \mathcal{S} quasi-equilibrium state [30], with only zero-quantum coherence (on the z -basis). Figure 2 shows the experimental results on 5CB. The data is organized so that the μ -axis displays the spectra of the different coherence orders n_c ($n_c = 0, \pm 1, \pm 2, \dots$). The spectrum of n_c order is symmetric to the one with $-n_c$ order, and the figure is arranged to show all the resolved coherence orders. The phase φ was varied in steps of 9.47 degrees in order to encode coherences with $|n_c| \leq 19$, however, spectra of coherences $|n_c| \geq 3$ have negligible intensity and are not shown. The τ -axis shows the spectra measured at increasing reversion times. In Figure 2 (a) the reversion block is a single MREV sequence where the total reversion time $\tau = 12\tau_1$ is varied by increasing the delays τ_1 (as shown in Figure 1(a)). The largest contribution corresponds to zero-order coherence

and, as expected, its spectrum is sinc-shaped (because of inevitable truncation of a zero frequency signal). A much lower amplitude single-quantum spectrum, observable at short times is seen to attenuate for $\tau \sim 400\mu\text{s}$. A similar behaviour is obtained in Figure 2 (b), where the reversion block is a series of concatenated MREV8 blocks with total length $\tau = n\tau_c$, where n is the number of blocks and the characteristic step-time is $\tau_c = 12\tau_1 = 90.36\mu\text{s}$. This sequence yields better results since the zero-order coherence amplitude has a much slower attenuation with τ , indicating a good reversion power, consistent with the ideal case calculated in the Appendix.

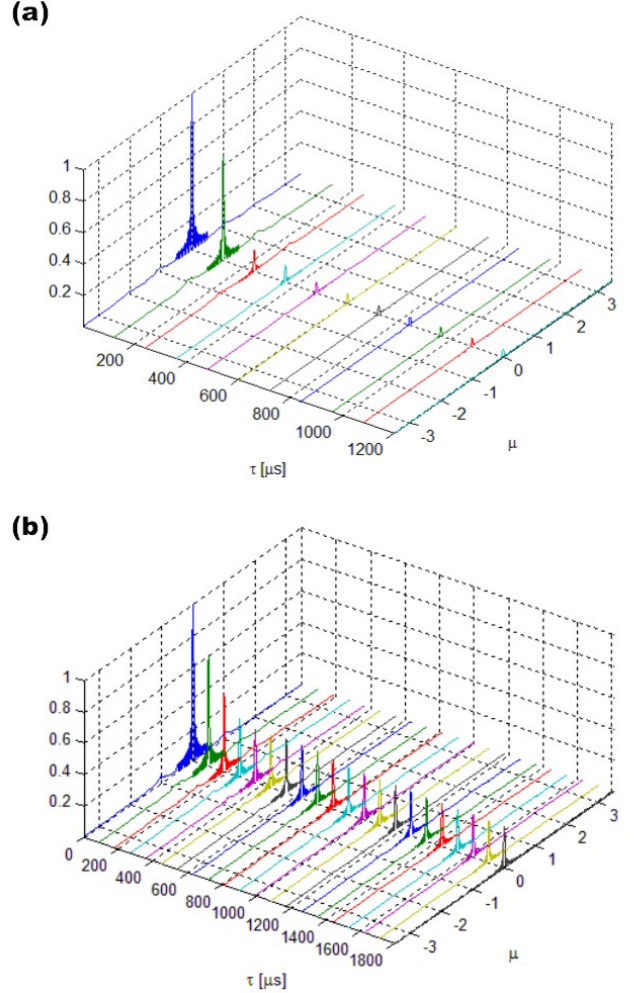


FIG. 2. Experimental spectra of the coherences measured in nematic 5CB. The time t_p is set to prepare the strong or \mathcal{S} -order ($t_p = 27\mu\text{s}$). The μ -axis shows a combination of spectra obtained for different coherence orders, that are symmetric with respect to zero order. Each coherence spectrum is limited to ± 25 kHz. The reversion block in (a) corresponds to a single MREV8 sequence where the total reversion time $\tau = 12\tau_1$ is varied in steps of $120\mu\text{s}$ by increasing the delays τ_1 ; in (b) we used an increasing number of short blocks with a characteristic step-time of $\tau_c = 90.36\mu\text{s}$.

A richer coherence spectrum is obtained by preparing the initial (\mathcal{W}) state with $t_p = 69\mu s$. In this case the zero-, single- and double-quantum coherence spectra are well distinguished, as shown in Figure 3. The amplitude of the zero-quantum coherence has a different dependence with τ under the two initial conditions. This behaviour is a consequence of the non-ideal performance of the reversion sequence, as shown in the Appendix A.

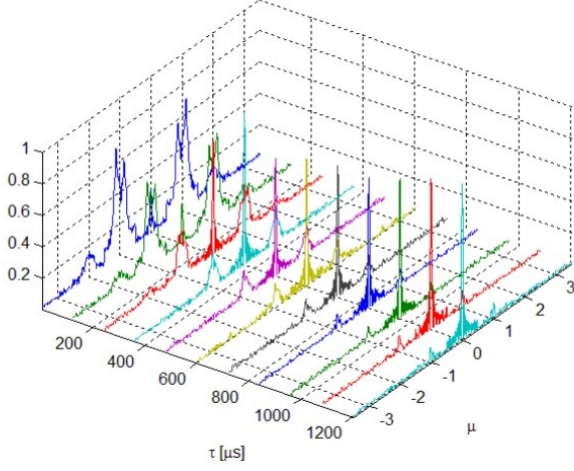


FIG. 3. Experimental spectra of the coherences measured in nematic 5CB. The time t_p is set to prepare the weak or \mathcal{W} -order ($t_p = 69\mu s$). The μ -axis shows a combination of spectra obtained for different coherence orders, that are symmetric with respect to zero order. Each coherence spectrum is limited to ± 25 kHz. The reversion block corresponds to a single MREV8 sequence where the total reversion time $\tau = 12\tau_1$ is varied in steps of $120\mu s$ by increasing the delays τ_1 .

The evolution of the multi-spin single-quantum coherence is worth to be analyzed separately: Figure 4(a) shows a stack plot of the single quantum spectra $\mu = 1$ obtained under the initial condition \mathcal{W} for different values of τ . Notice that, in terms of Eq. (49), the shape of these single quantum ($\nu_1 = 1$) spectra correspond to

$$\sum_{\Lambda_1 \lambda_1} g_{\lambda_1, \nu_1=1}^{\Lambda_1, \mathbf{x}}(t'_m) \mathcal{F}_t \left\{ \xi_{\lambda_1, \nu_1=1}^{\Lambda_1} \right\} (\omega, \tau, t_p).$$

It is then expectable that they differ from the NMR spectrum, which corresponds to the single-spin, single-quantum coherence $\lambda_1 = \Lambda_1 = 1$.

In order to display the frequency content as a function of the reversion time, Figure 4(b) shows several cuts of the amplitudes of the spectra at fixed frequency values, normalized to the corresponding values at $\tau = 0$. It can be seen that the higher frequency components decay faster than the low frequency ones, and that the characteristic decay times are noticeably different, the one of the higher frequency being approximately one third of that of the lower frequency. Previous work on 5CB [9] and 8CB

[11] gave a first indication that the attenuation the overall amplitude of the reverted single-spin, single-quantum signals is a consequence of irreversible decoherence. The results presented confirm that and also show that the higher frequency components are selectively attenuated while the quasi-equilibrium is developing.

The double quantum peaks have a much smaller amplitude than the multi-spin single quantum ones, just as happens with the calculated ones (see Appendix A), and their S/N ratio is too small to analyze the selective narrowing. However it can be seen that their amplitude decays monotonously with τ . It is worth to point out that this behaviour differs from the calculated one, since as shown in Figure 8(c2), the calculated amplitude of coherence ± 2 has the same trend as coherence 0. This difference indicates that the definite decay of this coherence observed in the experiment is due to a mechanism not accounted by the closed-system dynamics.

The behaviour of a sample of PAA_{d6} under the same reversion sequence (concatenated blocks) is shown in Figure 5, where (a) corresponds to a preparation time for the \mathcal{S} condition and (b) to the \mathcal{W} condition. The phase φ was varied in steps of 20.5 degrees. Again the \mathcal{W} condition gives rise to a richest coherence content. The amplitude variation of the zero-order coherence in both plots (a) and (b) can be explained by the inherent non-ideality of the reversion sequence (see Appendix A). A closer analysis of the selective attenuation of the multi-spin single-quantum spectra of PAA_{d6} is shown in Figure 6, where (a) contains a superposition of all the spectra at different reversion times τ , and (b) shows the τ dependence of the amplitude of different frequency components of the spectra obtained from (a). The data plotted in (b) is normalized in order to spot on their characteristic decay times. The dashed lines show the exponential decay fitting to each frequency component decay curve. The characteristic times depend on the frequency, being shorter for the larger frequency components, similarly to the case of 5CB.

In order to show that this characteristic behaviour is independent of the particular reversion sequence and compound, we carried out a similar experiment using the reversion sequence known as Magic Sandwich (MS) instead of MREV on the nematic liquid crystal 8CB. Figure 7(a) shows the multi-spin single-quantum spectra at different reversion times in 8CB, starting from the \mathcal{W} condition ($t_p = 72\mu s$). In this reversion sequence $\tau = 1.5 \tau_M$ as in Figure 1(c) [11].

The amplitude of the higher frequency components decrease with τ faster than the central peak. Figure 7(b) shows the τ dependence of the amplitudes of the central and side peaks. The central peak amplitude decay was fitted with a linear function with slope $\tau_d = 3.84\text{ms}$, while the characteristic decay time of the side peak (exponential fit) is $\tau_d = 1.24\text{ms}$.

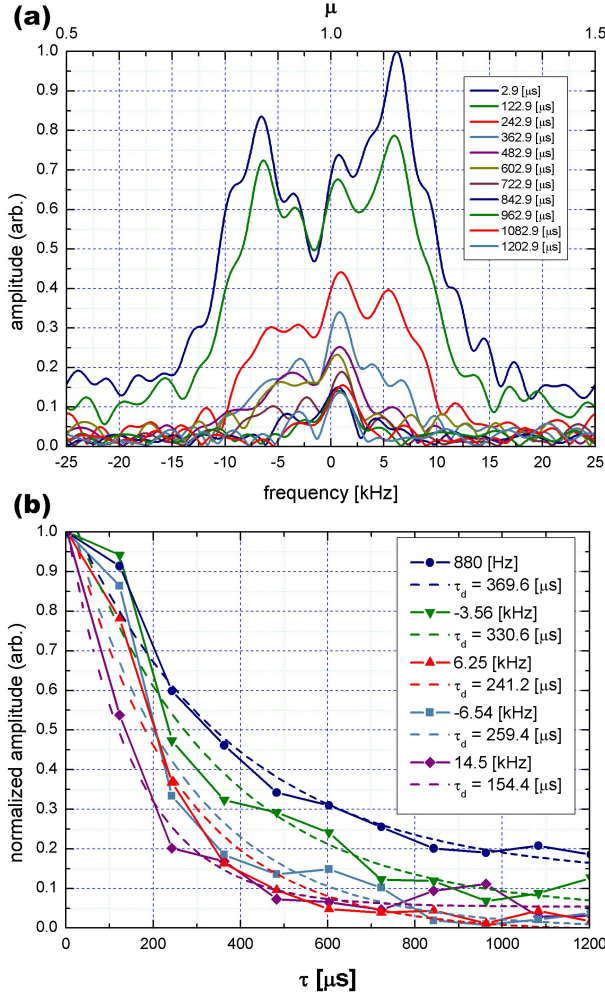


FIG. 4. (a) Front view of the spectra of coherence order $\mu = 1$ obtained in Figure 3 for nematic 5CB. (b) Time evolution of the (normalized) amplitude at different frequencies on the spectra of (a). The dashed lines are exponential fittings with different characteristic times as shown in the legend.

IV. DISCUSSION AND CONCLUSIONS

A wide variety of systems develop quasi-equilibrium states in an early time-scale, that is, in short times as compared with the lapse necessary to transfer a significant amount of energy to the environment. Once the system attains a quasi-equilibrium state, the dynamics of its spectroscopic properties can be described by a density operator that has the form of an expansion in quasi-invariants. There are many advantages in the use of a quasi-equilibrium description for theoretical as well as for practical analysis of the system dynamics. For example (i) representing the density operator in terms of a basis of quasi-invariants implies a very simple analytical representation that can be written as a linear combination of a few quasi-invariant operators; (ii) the fact that quasi-invariants are immune to decoherence, turns

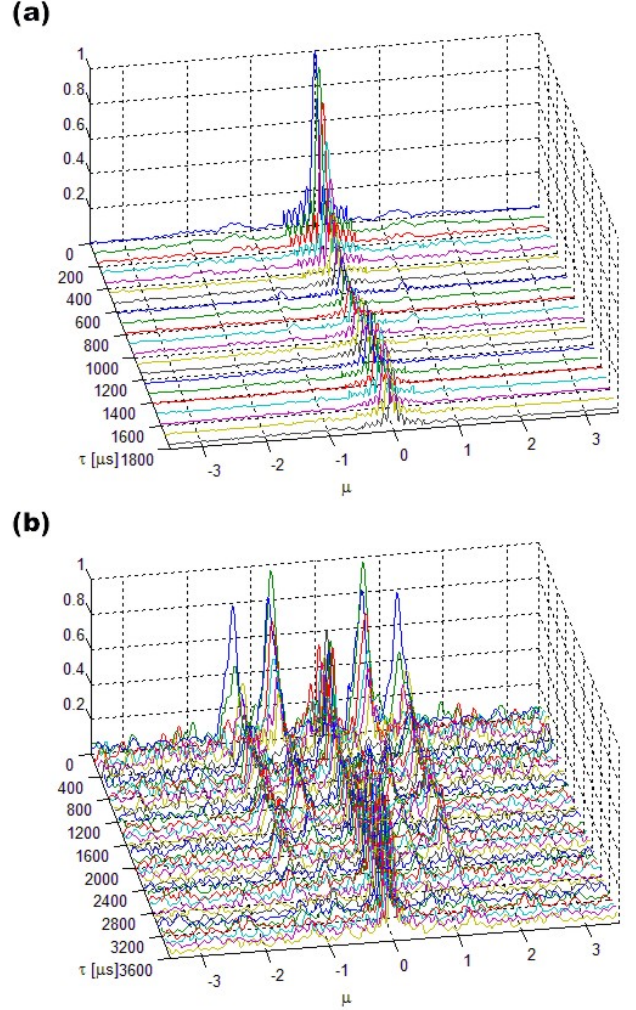


FIG. 5. Experimental spectra of the coherences measured in nematic PAA_{d6} at $T = 115^\circ\text{C}$, using blocks of MREV8 sequences of duration $\tau_c = 88.36 \mu\text{s}$, which define the τ axis step-times. The time t_p is fixed to set to prepare different dipolar quasi-equilibrium states, (a) Strong or \mathcal{S} -order ($t_p = 40 \mu\text{s}$), (b) Weaker or \mathcal{W} -order ($t_p = 84 \mu\text{s}$). The μ -axis shows a combination of spectra obtained for different coherence orders. In (a) each coherence spectrum is limited to ± 5 kHz and in (b) to ± 10 kHz.

them into good candidates to be used as memory units in quantum computations or to preserve information of the dynamics, etc.; (iii) since quasi-invariants only evolve by relaxation processes, they are very useful as sensors of the molecular motions and other long time scale effects of the environment over the spin dynamics. Therefore, an adequate understanding of the processes that bring the system toward the quasi-equilibrium states becomes essential.

In the literature on solid state NMR, the assumption is frequently made that the spin system can be considered as strictly closed in the early time-scale, and that the spin-lattice relaxation processes are the only channel by

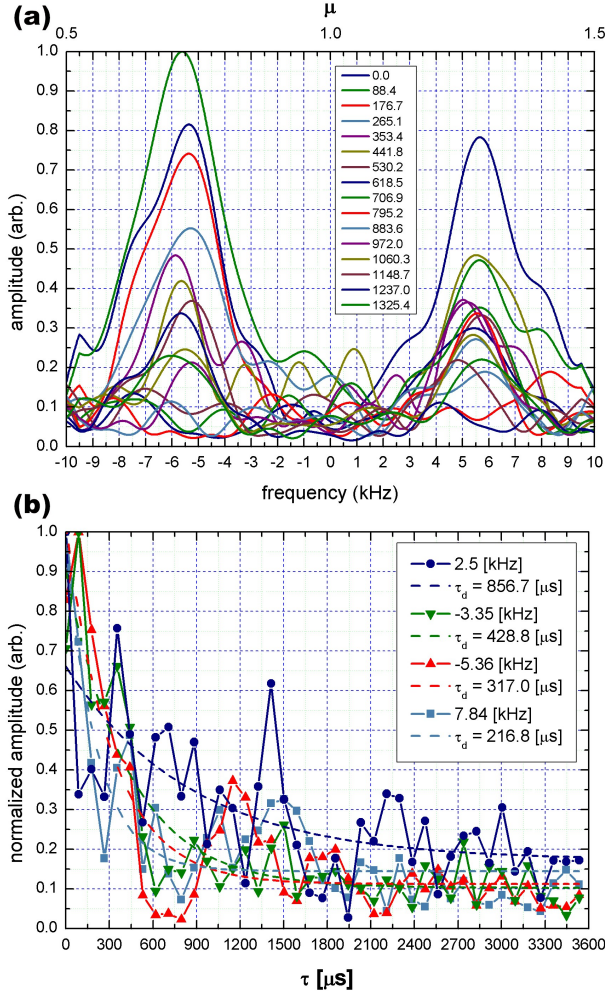


FIG. 6. (a) Front view of the single quantum spectra of nematic PAA₆₆ prepared in the W condition ($\mu = 1$ of Figure 5(b)), corresponding to $\tau < 1400 \mu\text{s}$. (b) Time evolution of the amplitude of different frequency components of the spectra obtained from (a). The curves were normalized to compare their decay rates. The dashed lines are the exponential fittings to each frequency component decay. Label indicates the characteristic decay times τ_d .

which the spin environment can act on the spin system [20, 31]. In this vision, the quasi-equilibrium state is not an actual state, but merely an apparent representation of the dynamics produced by the effect of a phase superposition from the spin variables, when an observable is measured. Following this vision, the decay of the spin observables when reversion experiment are performed is attributed either to imperfections in the experimental settings of the pulse sequences, or to the dissipative interaction among all the spins in the sample. Ideally, after improving the experimental techniques, the only limit to reversion would be some kind of ‘internal equilibration’ or ‘pseudothermalization’, a unitary process that would be the cause of the observed coherence decay. Although this

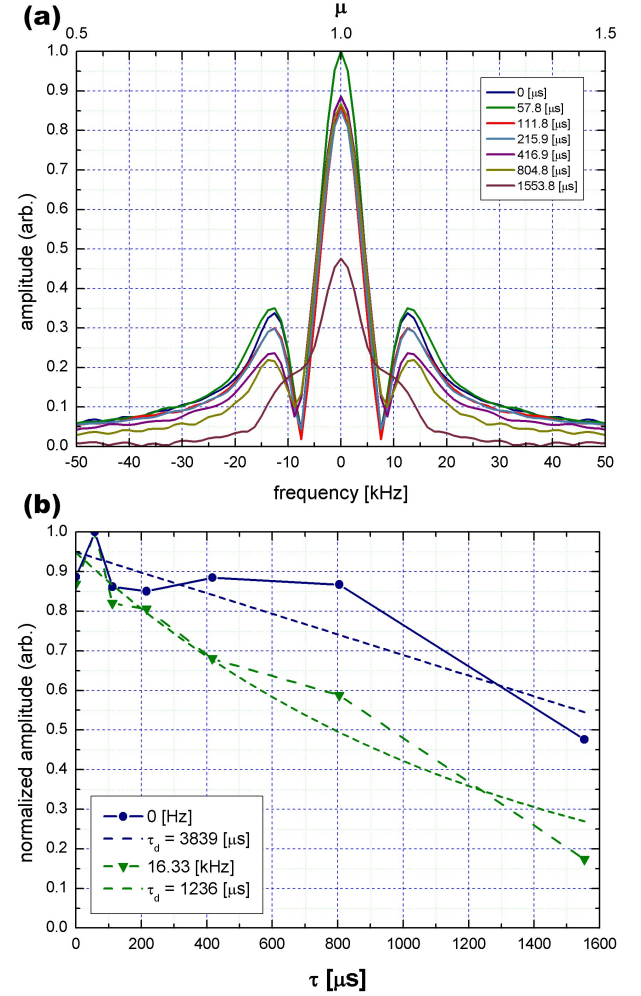


FIG. 7. (a) Stack plot of the spectra of the single quantum coherence in 8CB for different reversion times τ . (b) Time evolution of the (normalized) amplitude of the central peak (blue circles) and the side peaks (green triangles). The dashed lines are exponential fittings which show the marked difference in the characteristic decay times of the two frequency curves. The central peak amplitude decay was fitted with a linear function with slope $\tau_d = 3.84 \text{ ms}$.

line of thought might in principle give a phenomenologic explanation the observed signal attenuation in reversion experiments in solids, it cannot explain the phenomenon in liquid crystals. In the LC mesophases only the few spins which belong to each molecule are effectively interacting through their magnetic degrees of freedom, therefore the interaction among a thermodynamic number of spins cannot be claimed as the mechanism which inhibits longer experimental reversion times.

On the other hand, in the field of open quantum systems, the adiabatic decoherence due to the quantum interaction of the observed spin system and the reservoir is shown to be responsible of the decay of the matrix elements of the density operator [24, 25]. Particularly, in

references [8] and [9] the attenuation of single-spin NMR signals in reversion experiments on liquid crystals is explained under the formalism of open quantum systems. Such attenuation is essentially irreversible, even in the assumption of a perfect-reversion experiment. The characteristic behaviour of decoherence in an open quantum system is eigen-selectivity, which produces the characteristic frequency compression on the spectra of the coherences.

The importance of clarifying which class of spin system must be treated as an open quantum system in NMR experiments resides in the fact that spin systems are good candidates to be used as quantum registers, and in such case it is crucial to have longer decoherence times to allow the execution of a larger amount of quantum gates. Therefore, it is very important to know which description of the spin systems is more adequate, the closed or the open one, since it would lead to devising different encoding strategies. The results obtained in Section III contribute to this discussion. The experiment proposed in this work allowed monitoring the evolution of the multi-spin quantum coherences under a reversed spin dynamics. The single and double quantum coherece

amplitudes attenuate monotonously under different reversion schemes in a way that definitely differs from the evolution of a closed system under non-ideal experimental conditions. Besides, the frequency content of the multi-spin single-quantum coherence of the three studied compounds changes with the reversion time, showing that the higher frequency components attenuate faster than the lower ones. We interpret this results as an evidence of the occurrence of the eigen-selectivity effect during the transient from an initial state to the quasi-equilibrium state. This poses decoherence as the mechanism which drives a system to a QE state. Thus, we can conclude that the quasi-equilibrium states are actual states that the open quantum systems may attain during their transit to thermal equilibrium.

V. ACKNOWLEDGEMENT

This work was supported by Secretaría de Ciencia y Técnica, Universidad Nacional de Córdoba and MINCyT Córdoba. H.H.S. thanks CONICET for financial support.

-
- [1] P. Gennes and J. Proust, *The Physics of Liquid Crystals*, 2nd ed. (Oxford Univ. Press, Oxford, 1993).
 - [2] D. Shykind, J. Baum, S. Liu, A. Pines, and A. Garraway, *J. Magn. Reson.* **76**, 149 (1988).
 - [3] R. Dong, *Nuclear Magnetic Resonance of Liquid Crystals*, 2nd ed. (Springer Verlag, New York, 1997).
 - [4] R. G. C. M. Elroy, R. T. Thompson, and M. M. Pintar, *Phys. Rev. A* **10**, 403 (1974).
 - [5] H. Schmiedel, S. Grande, and B. Hillner, *Phys. Lett.* **91A**, 365 (1982).
 - [6] O. Mensio, C. González, and R. Zamar, *Phys. Rev. E* **71**, 011704 (2005).
 - [7] C. J. Bonin, C. E. González, H. H. Segnorile, and R. C. Zamar, *The Journal of Chemical Physics* **139**, 144907 (2013).
 - [8] H. Segnorile and R. Zamar, *J. Chem. Phys.* **135**, 244509 (2011).
 - [9] H. Segnorile and R. Zamar, *J. Chem. Phys.* **139**, 154901 (2013).
 - [10] W. Zurek, *Rev. Mod. Phys.* **75**, 715 (2003).
 - [11] C. González, H. Segnorile, and R. Zamar, *Phys. Rev. E* **83**, 011705 (2011).
 - [12] This designation, inspired in the name *einselection*, coined by W. Zurek to introduce environment induced superselection [10], was chosen to emphasize the fact that decoherence is governed by the spectral properties of the spin-environment interaction Hamiltonian. It is worth to notice that such dependence of decoherence on the interaction Hamiltonian has already been pointed out by Mozyrsky and Privman [25], who studied decoherence of a general quantum system coupled with environment modeled by a bosonic heat bath.
 - [13] J. Jeener and P. Broekaert, *Phys. Rev.* **157**, 232 (1967).
 - [14] H. Cho, D. Cory, and C. Ramanathan, *J. Chem. Phys.* **118**, 3686 (2003).
 - [15] The multiple quantum spectra could also be displayed by using time proportional phase increment [32]. Since we were not conditioned by the duration of the experiment we used another strategy to assure the frequency resolution needed.
 - [16] P. Mansfield, *J. Phys. C* **4**, 1444 (1971).
 - [17] W. Rhim, D. Elleman, and R. Vaughan, *J. Chem. Phys.* **58**, 1772 (1973).
 - [18] W. Rhim, D. Elleman, and R. Vaughan, *J. Chem. Phys.* **59**, 3740 (1973).
 - [19] W. Rhim, A. Pines, and J. Waugh, *Phys. Rev. Lett.* **25**, 218 (1970).
 - [20] W. Rhim, A. Pines, and J. Waugh, *Phys. Rev. B* **3**, 684 (1971).
 - [21] W. Rhim and H. Kessemeier, *Phys. Rev.* **B3**, 3655 (1971).
 - [22] H. Kessemeier and W. K. Rhim, *Phys. Rev.* **B5**, 761 (1972).
 - [23] M. Hohwy and N. Nielsen, *J. Chem. Phys.* **106**, 7571 (1997).
 - [24] V. Yukalov, *Laser Phys. Lett.* **8**, 485 (2011).
 - [25] D. Mozyrsky and V. Privman, *J. of Stat. Phys.* **91**, 787 (1998).
 - [26] A description of $\hat{U}_R(\tau)$, is presented in [8, 9] for MREV8-like sequences (see the Supplementary Material of [9] for a detailed expression of this operator). The effective evolution operator in the MS reversion sequence, is the same as described in [9].
 - [27] D. Weitekamp, *Adv. Magn. Res* **11**, 111 (1983).
 - [28] The total evolution operator $\hat{U}_T(t)\hat{U}_R(\tau)$ used in this work is equivalent to the total evolution operator described in Section II B of reference [9], this is $\hat{U}(t, t_2, t_1) = \hat{U}(t)\hat{U}_{rt}(t_2)\hat{U}(t_1)$, where the equivalences

between operators are $\hat{U}_T(t) \equiv \hat{U}(t)$ and $\hat{U}_R(\tau) \equiv \hat{U}_{rt}(t_2)\hat{U}(t_1)$ with $t_1 = \tau/(\kappa + 1)$ and $t_2 = \kappa t_1$ (κ is a positive constant whose value depends on the particular refocusing technique used, in our experiment $\kappa = 2$).

- [29] It is worth to note that the calculation of the coefficient (39) is different than the calculation of the expectation value in the references [8, 9], where the operator of the observable, in the total spin Hilbert space, is in a non-correlated form $\mathbf{1}^{(s_1)} \otimes \dots \otimes \mathbf{O}^{(s_i)} \otimes \dots \otimes \mathbf{1}^{(s_N)}$, which is not true for the tensorial operator in Eq. (34) and Eq. (39).
- [30] L. Buljubasich, G. Monti, R. Acosta, C. Bonin, C. González, and R. Zamar, *J. Chem. Phys.* **130**, 024501 (2009).
- [31] S. W. Morgan, V. Oganessian, and G. S. Boutis, *Phys. Rev. B* **86**, 214410 (2012).
- [32] D. Marion, M. Ikura, R. Tschudin, and A. Bax, *J. Magn. Reson* **85**, 393 (1989).
- [33] H. Segnorile, L. Barberis, C. González, and R. Zamar, *Phys. Rev. E* **74**, 051702 (2006).

Appendix A: Analysis of non-idealities in the spin-dynamics reversion sequence.

This appendix is dedicated to analyze the effects of non-idealities in the dynamics of the spins under the reversion sequence MREV8. In particular, we address the contribution of the non-secular terms in the dipolar Hamiltonian, which generally emerge when a period of unitary evolution under the dipolar Hamiltonian is enclosed between two pulses, as happens in the reversion sequences.

To mitigate the effects of the non-secular part over the dynamics, the free evolution time is usually set as small as possible, but not shorter than the irradiation time. However, this strategy does not apply when long reversion periods are needed.

We performed a numerical calculation of the signals produced by the experiment described in Section II, on

an 8-spin system having the geometry and dipolar couplings of the ^1H nuclei in a PAA_{d6} molecule [8]. The dynamics was calculated considering the spins as a closed system. In order to expose the effects of the non-secular dipolar terms, we calculated the outcome signals when the reversion sequence is a series of MREV8 blocks, we explored two different settings of the characteristic length τ_c of the individual blocks and their expected effect over different values of the preparation time t_p .

The graphs on left column of Figure 8 show the spectra corresponding to the condition $\tau_1 = 5\mu\text{s}$ and the left column to $\tau_1 = 20\mu\text{s}$. The first row corresponds to $t_p = 0$, or equivalently to reverting the FID (single-spin single-quantum signal); rows (b) and (c) correspond to preparation of the \mathcal{S} -order, and \mathcal{W} -order, respectively, and the preparation time in row (d) is an intermediate value between the former. The total reversion time in the τ axis is determined by the number of blocks.

Reversion is optimal when the characteristic time is small ($\tau_1 = 5\mu\text{s}$): the amplitude of each coherence is practically independent of τ throughout the range scanned (1 ms) in this simulation, as seen in Figure 8(a1), (b1), (c1) and (d1). On the contrary, a larger setting of τ_1 introduces variations on the amplitudes of the different spectra with the reversion time τ , as shown in (a2), (b2), (c2) and (d2). Particularly, the amplitude of the zero-quantum coherence peaks in (b2) and (d2), calculated in the closed system, show a slow attenuation similar to the one observed in Figure 2(a) and (b), as well as in Figure 5(a). When the initial state is prepared with $t_p = 97.5\mu\text{s}$, as in Figure 8(c2), the amplitude of zero-quantum coherence decreases and grows similarly to the experimental spectra of Figure 3 and that of Figure 5. The analysis indicates that this feature on the evolution of the zero-quantum coherence is just introduced by the non-reverted terms of pulse sequence and not due to the open character of the evolution.

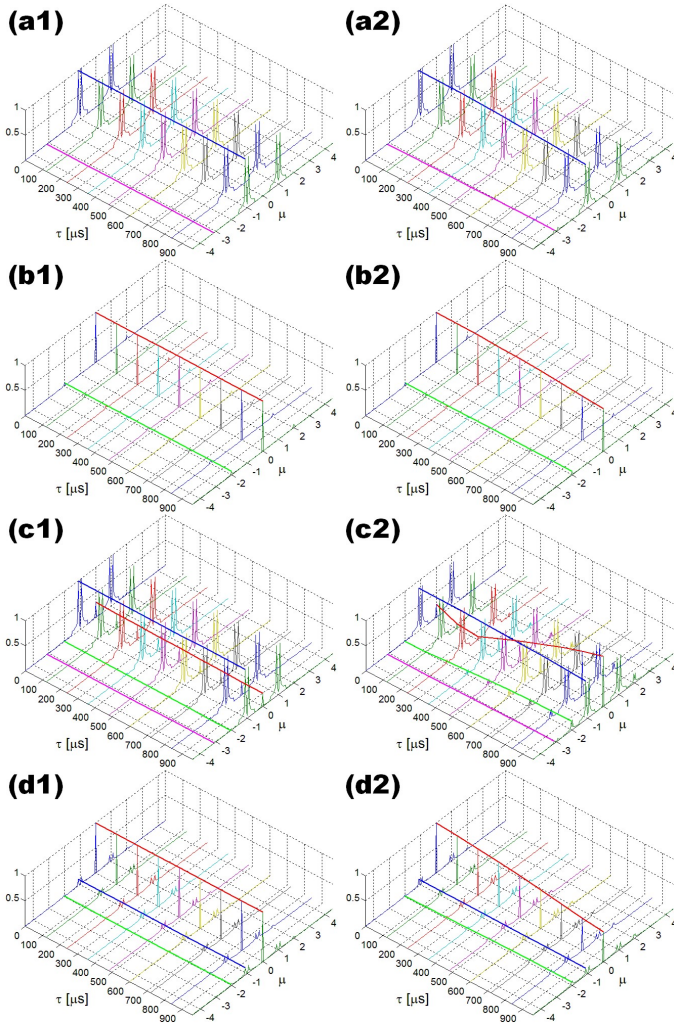


FIG. 8. Calculation of the proposed experiment for different preparation time, t_p , of the state of a PAA_{d6} molecule (dipole couplings from Ref. [33]). a1,a2: FID ($t_p = 0\mu\text{s}$), a1: $\tau_1 = 5\mu\text{s}$, a2: $\tau_1 = 5\mu\text{s}$. b1,b2: \mathcal{S} -order ($t_p = 47.5\mu\text{s}$), b1: $\tau_1 = 5\mu\text{s}$, b2: $\tau_1 = 20\mu\text{s}$. c1,c2: \mathcal{W} -order ($t_p = 92.5\mu\text{s}$), c1: $\tau_1 = 5\mu\text{s}$, c2: $\tau_1 = 20\mu\text{s}$. d1,d2: Mixed-state ($t_p = 195\mu\text{s}$), d1: $\tau_1 = 5\mu\text{s}$, d2: $\tau_1 = 20\mu\text{s}$. As a guide for visualizing the evolution over the time τ , solid lines are traced joining the maximum peak of the spectra of different coherences ($\mu = 0$ in red, $\mu = 1$ in blue, $\mu = 2$ in green, $\mu = 3$ in magenta).